Supporting Information

1. Calculation of flow rate:

Given that the flow detected by the MFC controller remains unchanged, the amount of gases introduced in the chamber stays constant. Based on the design characteristics of the inner tube of the MOCVD reaction, we proposed the following assumptions to calculate the average flow velocity of the vertical section passing through the center point of the samples:

a) The gas temperature above the growth zone in the inner tube is equal to the collection temperature at its end (150 °C);
b) Ignore any chemical reactions that lead to changes in gas volume, such as the decomposition of ammonia;
c) Use the vertical cross-sectional area at the center point of the substrate as the calculation basis, and use the gas flow rate at this cross-section to represent the average gas.

The specific steps are as follows, where V represents the gas flow rate through MFC and stands for the sum of RUN, MO precursor, NH_3, and Carrier gas. Then the flow rate can be simply calculated as:

$$v = V/S \tag{S1-1}$$

S is the vertical cross-sectional area at the midpoint of the inclined graphite support in the inner tube. As the gas pressure and temperature changed during the actual reaction process, so it is necessary to take a conversion based on the Ideal Gas Law.

$$PV = nRT \tag{S1-2}$$

Then the actual gas flow rate V_t can be obtained, as described in the following equation, where P_1 is 3 times atmospheric pressure, T_1 is 273K, T_s is the inner tube gas temperature, and P_s is the reaction chamber pressure:

$$V_t = VP_1T_s/(SP_sT_1) \tag{S1-3}$$

The calculation results indicate that the gas flow rate in the experimental group can reach a speed from 7.48 to 37.38 $m{\cdot}s^{-1}$.

2. SEM images of different growth time under 30 torr.

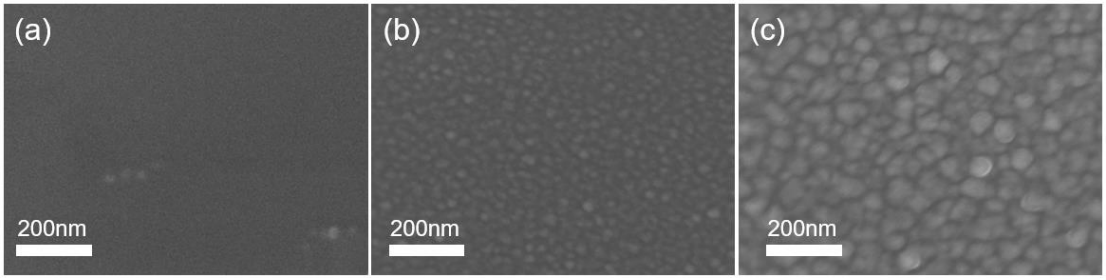

Fig. S1(a)-(c): SEM surface morphology of ZrN film deposited for 15min, 30min and 1h, respectively.

3. Calculations related to XRD

i) The interplanar spacing $d_\perp$ can be calculated according to Bragg's formula, where λ represents the Cu $K\alpha_1$ wavelength and equals to 1.54056 Å.

$$2d_\perp sin\theta = n\lambda \tag{S3-1}$$

θ is the half of Bragg diffraction angle, and $n = 2$ is the diffraction order which corresponding to the (200) crystal plane. According to the lattice structure relationship of the cubic crystals, the lattice parameter $a_\perp$ in this direction can be calculated through the following formulas.

$$d_\perp = \frac{a_\perp}{\sqrt{h^2+k^2+l^2}} \tag{S3-2}$$

ii) The texture coefficient (TC) was also calculated to estimate the preferred orientation of the film defined as the following formula, where $I_{(hkl)}$ is the integrated intensity of the corresponding (hkl) peak by conventional θ/2θ scan, ranging from 2θ = 10 to 90° with a sampling step of 0.02° and scanning rate 0.2°/s.

$$TC = {I_{(hkl)}}\Big/{\sum I_{(hkl)}} \tag{S3-3}$$

iii) The thermal mismatch stress in ZrN films could be calculated as 1.88 GPa (tensile) by the following formula, with the assumption that the thermal expansion coefficients are constant.

$$\sigma_{th} = \frac{E}{1-v_f}\int_{T_1}^{T_2}(\alpha_s - \alpha_f)\,dT \tag{S3-3}$$

4. Binding energy of Zr 3d and N 1s of the ZrN film deposited under 30 torr by XPS.

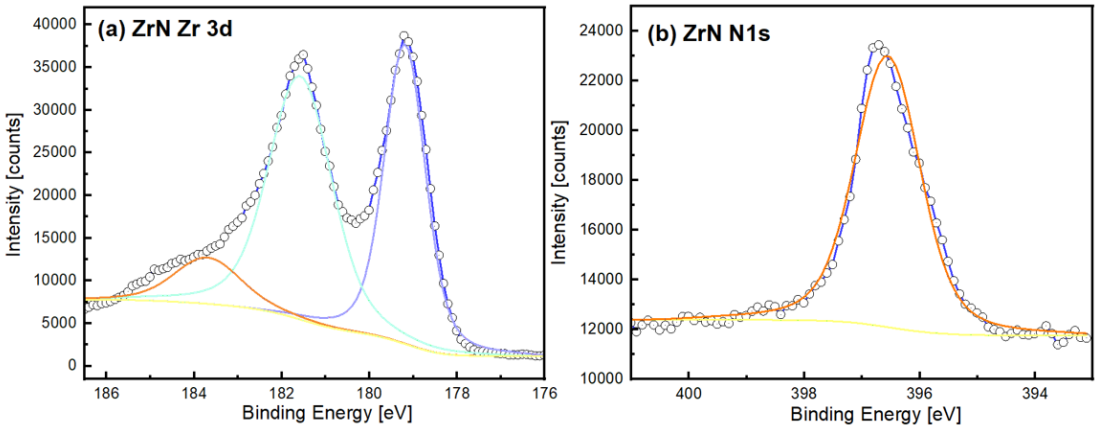

Fig. S2: Binding energy of Zr 3d and N 1s of ZrN films.

The peaks at 179.3 eV and 181.7 eV in Zr 3d correspond to Zr 3d5/2 and Zr 3d3/2 of ZrN, respectively, and also show an energy interval of 2.4 eV. Another broad peak originates from O-Zr-N and is related to surface oxidation during storage under natural conditions. N 1s located at 396.7 eV was also derived from the N-Zr bond. Furthermore, the N/Zr ratio was evaluated at 0.96 from the semi-quantitative results of atomic content.

5. In-depth analysis of the ZrN film by XPS.

Tab. S1 Atomic % (%) of ZrN film by XPS.

Etch Time /s	Si 2p	Zr 3d	C 1s	N 1s	O 1s	N/Zr
0	0.00	18.12	29.39	7.88	44.61	0.44
150	0.00	45.24	0.00	43.80	10.95	0.97
300	0.00	44.80	0.00	44.89	10.31	1.00
451	0.00	45.04	0.00	45.08	9.89	1.00

601	0.00	45.43	0.00	44.68	9.89	0.98
751	0.00	45.82	0.00	44.43	9.75	0.97
826	0.00	45.01	0.00	45.01	9.98	1.00
901	0.00	45.20	0.00	44.83	9.97	0.99
976	0.00	44.12	2.47	43.98	9.43	1.00
1051	0.00	45.31	0.00	44.19	10.51	0.98
1126	0.00	44.23	2.38	43.46	9.93	0.98
1202	0.00	45.76	0.00	43.98	10.26	0.96
1277	1.81	44.93	0.00	43.07	10.19	0.96
1352	1.99	44.26	0.00	43.14	10.61	0.97
1427	2.07	43.94	2.69	42.09	9.21	0.96
1502	3.31	44.06	0.00	42.60	10.03	0.97
1577	5.94	43.13	0.00	41.51	9.43	0.96
1652	14.55	38.14	0.00	38.41	8.90	1.01
1727	28.16	31.51	0.00	32.35	7.97	1.03
1802	49.62	22.46	0.00	22.17	5.74	0.99
1877	67.74	13.82	1.67	12.65	4.12	0.92
1952	82.87	8.12	0.00	6.34	2.66	0.78
2028	89.95	4.70	0.00	3.18	2.17	0.68
2103	93.42	3.20	0.00	1.36	2.03	0.42
2178	95.52	2.13	0.00	0.00	2.34	0
2253	96.14	1.87	0.00	0.00	1.99	0
2328	95.97	1.79	0.00	0.00	2.23	0
2403	96.38	1.44	0.00	0.00	2.18	0

6. The refractive index n and extinction coefficient k in the wavelength of 200-1600 nm of bare Si.

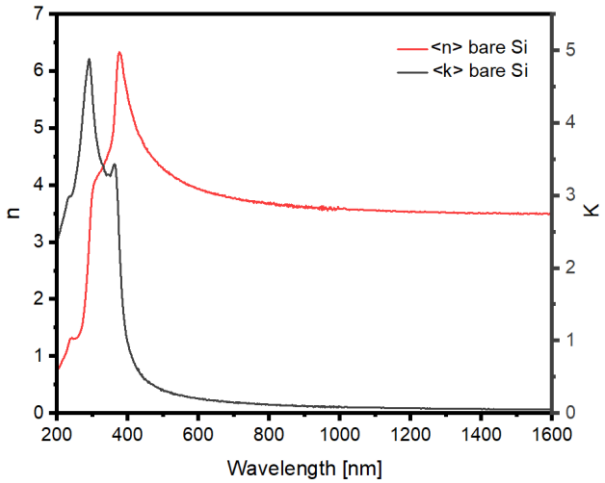

Fig. S3: The refractive index n and extinction coefficient k in the wavelength of 200-1600 nm of bare Si substrate.